EurJIC European Journal of Inorganic Chemistry
ChemPubSoc Europe
FULL PAPER

DOI:10.1002/ejic.201500164

Facile Synthesis of (110)-Plane-Exposed Au Microflowers as High Sensitive Hydrogen Peroxide Sensors

Fengjiao Yu,[a] Zhong Liu,*[a,b] and Wuzong Zhou*[a]

Keywords: Gold / Electron microscopy / Microflowers / Nanostructures / Crystal growth / Biosensors

A flower-like Au microstructure with a dominantly exposed active (110) plane has been prepared by a simple, facile method at room temperature. Various experimental factors that can control the shape of the Au microflowers have been investigated and optimized. Furthermore, the glassy carbon electrode modified with these Au microflowers exhibits high electrochemical activity towards H_2O_2 reduction. The sensor shows a linear range from 10 μM to 5.53 mM with a detection limit of 2 μM, which can be attributed to the exposed (110) planes and 3D hierarchical structure of the Au microflowers.

Introduction

H_2O_2 is a general product of oxidases in a number of biological enzymatic processes in vivo,[1] and its level closely correlates to states of aging and other diseases such as diabetes and cancer.[2] Besides, H_2O_2 is a kind of mediator applied in pharmaceutical, environmental and clinical research as well as in the food industry.[3] Therefore, developing reliable detecting methods of H_2O_2 down to trace levels are practically important and have attracted considerable interest. Electrochemical H_2O_2 sensing is a promising technique, which is highly sensitive, accurate and rapid. One widely used approach is to immobilize an enzyme, normally horseradish peroxidase (HRP), onto electrodes.[2,4] However, with regard to the high cost, difficulty of activity retention and short lifetime of the immobilized enzyme, it is important to develop efficient enzyme-free strategies for H_2O_2 detection.

Recently, various materials, such as Pd nanoparticles plated on a Si substrate,[5] carbon nanotubes/Ag nanohybrids[6] and MnO_2 nanoparticles[7] have been reported to work effectively in the non-enzymatic detection of H_2O_2. Although these materials exhibit a good performance as a biosensor, some of them are toxic or harmful to biological systems so that they are not suitable for application in vivo. In contrast, Au metal is rather safe and very promising for use in living organism because of its biocompatibility.

On the other hand, the morphology of materials can strongly influence their properties. Three-dimensional (3D) hierarchical metallic materials with unique structural characteristics, such as high surface area, fast mass transfer or diffusion, can exhibit improved performance.[8] Therefore, Au with a 3D hierarchical structure is a potential candidate for the non-enzymatic detection of H_2O_2.

Au and its hybrids applied as enzyme-free H_2O_2 sensors have attracted much attention recently. For example, electrodes modified with Au spheres assembled by nanowires detect H_2O_2 on successive injection of 0.1 mM H_2O_2.[9] Au nanoplates have been used as a H_2O_2 detectors with concentrations from 0.1 to 50 mM.[10] Some Au-based composites, for example, Au-nanoparticle/polyoxometalate/graphene hybrids have a low detection limit and wide linear range,[11] but this tricomponent composition may increase the cost of materials. Single-component Au particles exposed with highly active planes may perform well and be economic candidates for enzyme-free biosensors.

Herein, we report a one-step method for the room-temperature preparation of Au microflowers, which is simple and facile to produce uniform, (110)-exposed Au particles with a 3D construction. The Au microflower-modified electrode has been used as a sensor for the non-enzymatic detection of H_2O_2 in 0.01 M phosphate-buffered saline (PBS, pH 7.2) and exhibits an enhanced sensitivity than commercial Au electrodes, as well as good linearity in a wide range and with a low detection limit down to 2 μM H_2O_2.

Results and Discussion

Structure and Morphology

The Au microflowers were successfully prepared at room temperature by using ascorbic acid as a reducing agent. Fig-

[a] School of Chemistry, University of St Andrews, St Andrews, KY16 9ST, United Kingdom
E-mail: wzhou@st-andrews.ac.uk
http://www.st-andrews.ac.uk/chemistry/
[b] Key Laboratory of Salt Lake Resources and Chemistry, Qinghai Institute of Salt Lakes, Chinese Academy of Sciences, Xining 810008, China
E-mail: liuzhong@isl.ac.cn
Supporting information for this article is available on the WWW under http://dx.doi.org/10.1002/ejic.201500164.

ure 1a is a low-magnification scanning electron microscopic (SEM) image of the microflowers, which indicates the quite uniform size of particles with a diameter of about 1 μm. The hierarchical structure of each microflower is composed of several nanoflake-like petals that are ca. 50 nm thick, as shown in Figure 1b. The high-resolution transmission electron microscopy (HRTEM) analysis (Figure 1c), the XRD pattern (Figure 1d) and energy-dispersive X-ray spectroscopy (EDX) (Supporting Information, Figure S1) confirm the face-centred cubic (fcc) phase of Au.

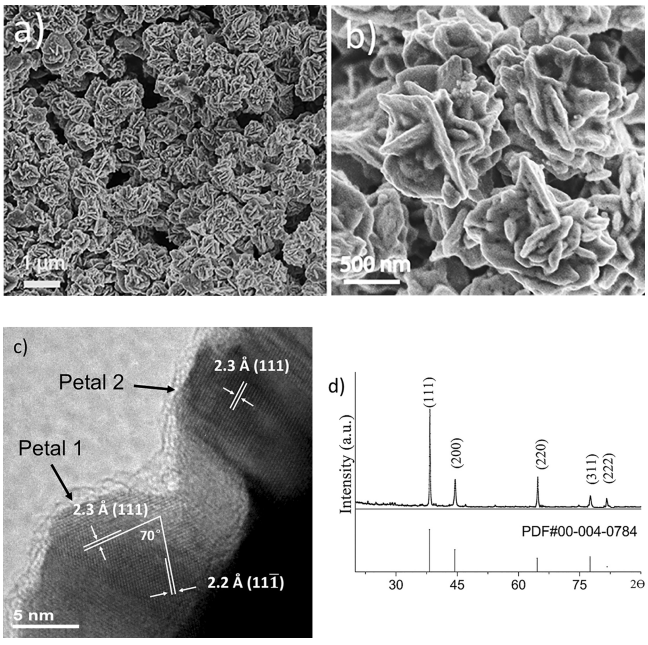

Figure 1. a) and b) SEM images of the Au microflowers with different magnifications. c) HRTEM image showing fringes of the (111) planes in two different petals. The exposed facets of the petals are (110) as detected from petal 1. d) XRD pattern of the Au microflowers that can be indexed to the pure face-centred cubic phase (PDF 00-004-0784). The weak peaks result from background noise and some possible impurities, which are not identified.

In Figure 1c, the lattice fringes observed on the petals can be well indexed to the {111} planes of Au. In particular, the two-dimensional fringes in petal 1 can be indexed to the (111) and (11$\bar{1}$) planes, with an interplane angle of 70°. The normal direction to the dominantly exposed crystal planes is the [$\bar{1}$10] axis, which is coincident with the electron beam. Therefore, the exposed surface facing us, of this petal, is the ($\bar{1}$10) plane. The electron microscopy results of many particles reveal that the most popular surface of the petals terminates by the {110} planes.

It is noted that, although the highest peak in the XRD pattern is (111), the relative intensity of the (220) peak in the XRD pattern (Figure 1d) is significantly higher than those from decahedral Au particles with {111} facets[12] and from Au spherical particles.[13] The intensity of diffraction and the exposed surface of particles are two different aspects. The strongest diffraction peak does not have to be the exposed plane, e.g. the whole surface of icositetrahedra of zeolite analcime is formed by only 24 {211} exposed facets, but the XRD peak of the highest intensity is (400).[14] On the other hand, the exposed surface and the morphology of crystals will affect the relative intensity of the XRD peaks, i.e. the ratio of the peaks.

Figure 1c also reveals that the two petals have different crystallographic orientations, which is consistent with the selected area electron diffraction (SAED) results that these microflowers are actually polycrystalline (Supporting Information, Figure S2). The outmost layer with low-contrast on the petals in Figure 1c is likely polyvinylpyrrolidone (PVP) surfactant absorbed on the Au surfaces. This synthetic method proves to be facile and effective to prepare uniform Au microflowers.

In a typical synthesis, the Au microflowers were produced in the presence of polyvinylpyrrolidone (PVP) and KBr in acidic solution. In order to investigate the effect of different synthetic parameters, various preparations were carried out.

KBr appears to be one of the key chemicals for the formation of the flower-like morphology. Reduction in the amount of KBr from 120 mg (under typical conditions) to 30 mg (see Experimental Section) resulted in less shape-controlled products, which contained about 40% microflowers and 60% spherical particles, as shown in Figure 2a. The products became almost entirely spherical in the absence of KBr, as displayed in Figure 2b. According to Wang et al.,[15] Br^- can absorb on the Au {110} surfaces and transfer charges to the surface Au atoms, which stabilizes the {110} facets. In the XRD pattern shown in Figure S3 (Supporting Information), the relative intensity of the (220) peak decreases significantly when the amount of KBr was reduced, while the intensity of the (311) peak increases. The changes in the intensity of the XRD peaks with variation in KBr provide evidence that Br^- can stabilize the Au {110} planes.

PVP has a significant but different role. Figure 2c displays a SEM image of the particles prepared in the absence of PVP, large aggregates were formed with sizes ranging from 4 to 7 μm. PVP, acting as a capping agent, can adsorb on the metal surfaces and protect the particles from attaching together.[16] Too fast and tight aggregation of the nanocrystallites without the use of PVP might alter the environment for the development of individual Au plates. Therefore, PVP is indispensable in stabilizing individual Au microflowers and narrows the size distribution.

Addition of HCl can change the acidity of the reaction system and can strongly affect the size of the Au microflowers. Figure 2d is a SEM image of the Au microflowers prepared in the absence of HCl. The products retain the flower-like morphology, while the size of the Au microflowers decreases to 0.3–0.5 μm and become less uniform. This is because ascorbic acid acts as the reducing agent by the following reaction: $C_6H_8O_6 \rightarrow C_6H_6O_6 + 2H^+ + 2e^-$.

Without the addition of HCl, the pH of the system is high and the reduction of the metal ions will be rapid,[17] which leads to the formation of more Au seeds and finally smaller particles. On the other hand, adding more HCl or more ascorbic acid did not change the morphology of the Au microflowers (Supporting Information, Figure S4) as

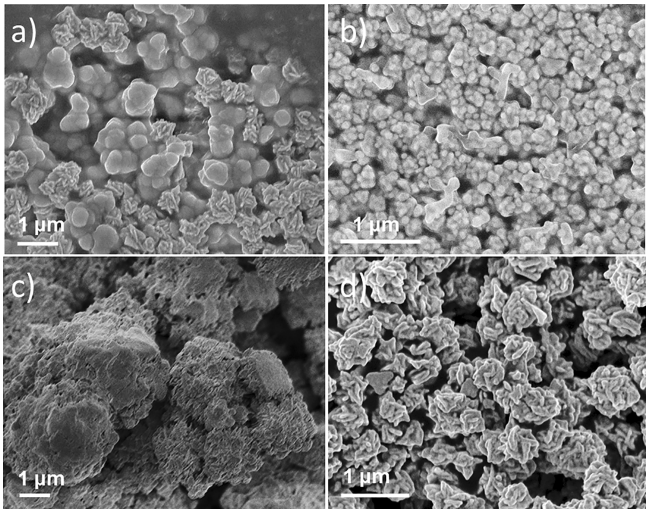

Figure 2. SEM images of the Au particles synthesized under different reaction conditions: a) in the presence of less KBr (30 mg), resulting in some spherical particles; b) in the absence of KBr, resulting in only spherical product; c) in the absence of PVP, producing large aggregates; and d) in the absence of HCl, producing smaller Au microflowers.

both agents are in excess under the current synthetic conditions.

Intermediate products were also studied to investigate the growth process. Figure 3a is a SEM image of the 8 min product, which already shows the flower-like shape of the particles, but with a smaller number of petal flakes. This indicates that some relatively large plates form first and act as the base for growth of the petal flakes, which occurs at a later stage. The 15 min product in Figure 3b has a larger average particle size (≈700 nm) in comparison with the 8 min sample (≈400 nm) and contains more petal flakes in each particle. The microflower particle size in the 15 min sample, however, is still smaller than that in the final product with an average diameter of 1 μm. This indicates that the Au atoms would continuously deposit on the particles. Consequently, a mechanism of self-assembly of pre-formed large petals to construct flower-like particles can be ruled out.

In a typical synthesis, the reaction took place at room temperature and proceeded too fast to capture the very early stage products. The reaction was then carried out in an ice bath to extract the initial intermediates. The sample collected after 5 min in the ice bath contains petal-free plates with sizes of about 200 nm (Figure 3c), as well as some smaller particles that might develop into plates after a longer reaction time. The plates are single crystals with exposed {110} surfaces, indicated by the electron diffraction pattern as shown in Figure 3d. From the surface-energy point of view, the {111} facets of Au are the most densely packed so are more stable. The presence of the {110} facets in the Au microflowers can be attributed to the addition of Br^- ions and PVP. The former can bind with the {110} facets, transfer charges to the surface Au, which makes the atomic arrangement on the {110} surface more stable.[15] PVP can also absorb on the {110} facets, which enhances surface reconstruction into a "saw-tooth" structure when viewed along some strips, as a result of missing atomic columns, as previously observed.[15] It is believed that the formation of these strips, with small regions of {111}, can significantly reduce the lattice energy of the Au {110} surface.

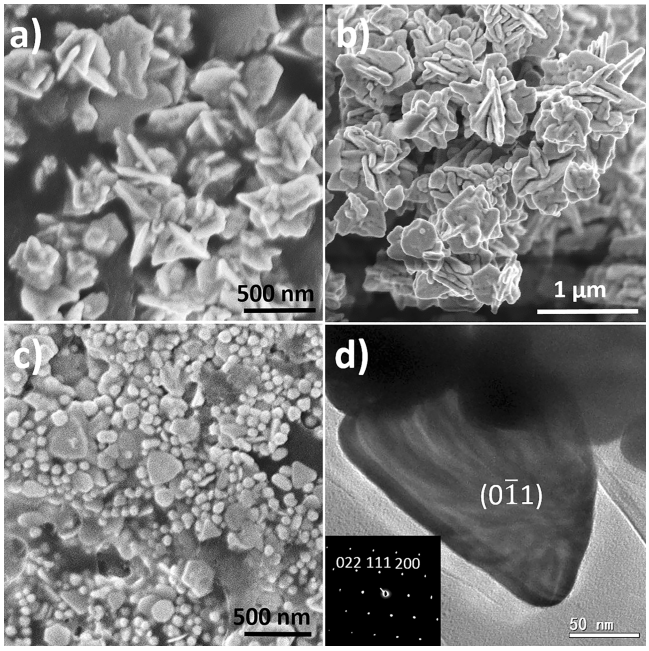

Figure 3. SEM images of the Au particles collected after a) 8 min, b) 15 min at room temperature. c) SEM and d) TEM of the Au plates formed after 5 min reaction in an ice bath. Inset of d) is the corresponding SAED pattern viewed along the [0$\bar{1}$1] zone axis.

On the basis of the above observations, a plausible mechanism is illustrated in Scheme 1. We observed that nanoplates of Au, with surfaces terminated with the {110} planes, form at an initial stage (I), which then serve as bases for the attachment of petal flakes (II).

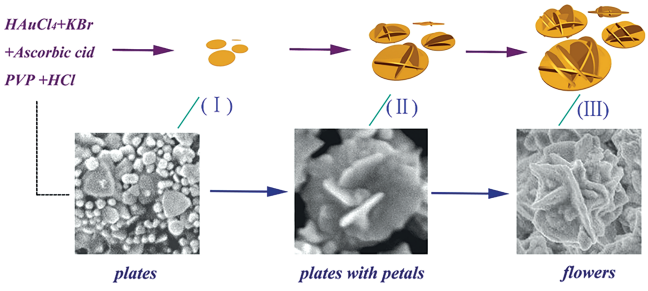

Scheme 1. Illustration of the morphology evolution process of the Au microflowers: (I) formation of smooth plates; (II) petal flakes start to grow on both sides of the plates; (III) further growth of petals produce flower-like particles.

The driving force of the attachment of petal flakes is still not fully understood. The connection of petals on the plate surface most likely takes place in the defect areas on the surface. The Non-oriented manner of the attachment revealed in the present work indicates that the petals do not grow directly from the crystal surface of the nanoplates. It

may follow a mechanism of attachment of Au nanocrystallites with random orientations on the plate surface with a PVP layer[18] and then extend the crystals to have a crystalline interface between the plate and petals. Most petals vertically stand on the plate surface. The faces of both the plates and petals are covered by PVP and Br^-, so attachment of the particles in a face-to-face way becomes difficult. Consequently, edge-to-face is the favourite connection manner. Since the properties of both surfaces of the nanoplates are the same, attachment of the petals occurs on both surfaces. The flower morphology appears at very early stage when the particle sizes are small. The mini-flower Au particles act as seeds and grow larger continuously through an Ostwald ripening process. After prolonged reaction time, flower-like products are formed with 3D hierarchical structures (III).

Previous reports have proposed that the flower-like morphology may be caused either by single-crystal growth and preferentially oriented along one direction in ZnO flowers[19] or by radical assembly of simultaneously formed large plates of BiOBr microflowers.[20] The formation mechanism of the Au micro-flowers in the present work is different from any established mechanism.

Amperometric Detection of Hydrogen Peroxide

Noble metal particles have attracted much attention because of their astounding properties and numerous possibilities in sensing.[21] In particular, Au-based particles are potential candidates for enzyme-free biosensors.[22] In this work, the prepared microflower Au specimens were found to have a good response for the enzyme-free detection of H_2O_2 at a concentration level as low as 2 μM, as shown in the amperometric response in Figure S5 (Supporting Information).

Figure 4 shows a typical cyclic voltammogram of the Au-microflower-modified GC electrode, commercial gold electrode and bare GC electrode in 0.01 M phosphate-buffered saline (PBS, pH 7.2) in the presence of 0.3 mM H_2O_2. It shows that the Au microflower electrode performs the best. At a potential near –0.2 V (vs. SCE) for H_2O_2 reduction, the current of the bare GC electrode is –1.09 μA, and current increases to –1.60 μA as the working electrode is changed to a commercial gold electrode. When we used the prepared gold microflowers to modify the GC electrode, the current reached –1.97 μA, which is much higher than that of the bare GC and commercial gold electrode with the same diameter.

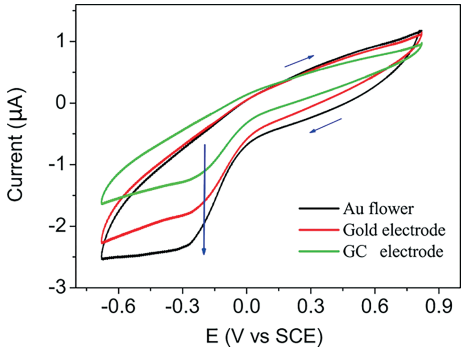

Figure 4. Cyclic voltammograms of Au-microflower-modified GC electrode, commercial gold electrode and bare GC electrode in 0.01 M PBS (pH 7.2) in the presence of 0.3 mM H_2O_2. Scan rate = 20 mV/s.

The sensitivity of the Au-microflower-modified GC electrode was further investigated by amperometric response, as shown in Figure 5. The *i*–*t* curves in Figure 5a were recorded at –0.2 V (vs. SCE) in 0.01 M PBS (pH = 7.2). It is obvious that the Au microflower sample (curve A) has the largest current response toward H_2O_2 sensing. Whereas, commercial gold and bare GC electrode present low sensing performance as shown in Figure 5a, especially at low concentration of H_2O_2. The amperometric response of the Au microflower sample at higher H_2O_2 concentrations is presented in Figure S6 (Supporting Information). On the basis of the *i*–*t* curves, the current as a function of concentration plots were obtained and are shown in Figure 5b; a good linear relationship is found. The Au microflower structurally modified GC electrode has a linear region ranging from 10 μM to 5.53 mM with a high correlation coefficient of 0.998.

We have compared the performance of our Au microflowers and other Au nanoparticles or Au-based composite electrodes in Table S1 (Supporting Information). Our gold

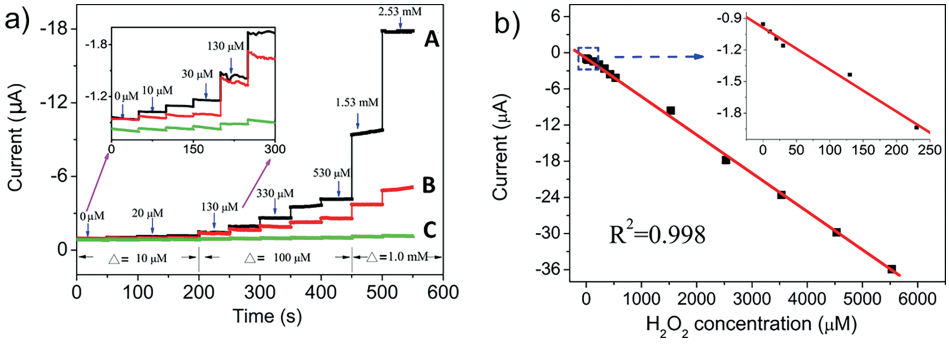

Figure 5. a) Amperometric response of A) Au-microflower-modified GC electrode B) commercial gold electrode and C) bare GC electrode, with successive addition of H_2O_2 in 0.01 M PBS (pH = 7.2) at an applied potential of –0.2 V (vs. SCE) (inset: high-resolution plot of first 300 s). b) Calibration curves of Au-microflower-modified GC electrode (inset: high-resolution plot of first 230 μM).

microflowers exhibit a higher sensitivity compared to Au nanoplates[10] with similar dimensions, and a wider linear range compared to the Au ternary composites listed, which make the Au microflower a promising candidate component for composite materials in H_2O_2 biosensing. In addition, the microflowers show good stability. After repeating the test 10 times, the CV curves remain unchanged and the structure of the microflowers remains intact, as shown in Figure S7 (Supporting Information).

The exposed (110) planes and flower-like morphology are responsible for the good performance. Firstly, the high-energy (110) surfaces likely expose more active sites to combine with the target molecules, which is critical to the high-sensing performance because the electrochemical reaction takes place on the surface of the solid phase. Secondly, the excellent performance of the Au microflowers could be attributed to the 3D hierarchical structure, which can facilitate electron transfer.[23]

Conclusions

We have demonstrated a simple, one-step method to prepare uniform Au microflowers with the exposed {110} surfaces at room temperature. Although rhombic dodecahedral Au particles with 12 {110} facets have been synthesized by using *N*,*N*-dimethylformamide,[24] the microflowers consisting of nanoplates with two (110) facets have even larger specific surface areas. The synthetic conditions, such as the concentrations of PVP, KBr and HCl were investigated and optimized to obtain high-quality Au flower-like particles. The growth process was also investigated, and a plausible mechanism was proposed. The Au-microflower-modified GC electrode shows a linear relationship for H_2O_2 detection in the range from 10 μM to 5.53 mM with a limit of 2 μM. This work demonstrates the superior electrocatalytic activity of the hierarchical Au flower-like structure and provides prospects for the design of enzyme-free electrochemical H_2O_2 sensors.

Experimental Section

Synthetic Method for the Au Microflowers: In a typical preparation, polyvinylpyrrolidone (PVP, 60 mg) and KBr (120 mg) were dissolved in H_2O (1 mL), and then mixed with HCl solution (2 mL of a 1 M solution) and $HAuCl_4$ solution (2 mL of a 30 mM solution). Under vigorous stirring, ascorbic acid (105 mg) dissolved in water (3 mL) was added dropwise into the solution. After reaction for 24 h at room temperature, the product was collected by centrifugation and washed several times with acetone to remove residual reactants. The amount of PVP, KBr and HCl were varied to study their effects on the synthesis. The initial growth process is very rapid. In order to study the early growth stage of the Au microflowers, an ice bath was used, and the products were collected after reaction for 5 min at low temperature.

Characterization: The morphology of the Au microflowers was examined by field-emission gun SEM on a JEOL JSM–6700F microscope operating at 2–5 kV. Powder X-ray diffraction (XRD) was performed on a PANalytical Empyrean diffractometer with Cu-K_α radiation. HRTEM images and SAED patterns were obtained on a JEOL–2011 electron microscope operating at 200 kV equipped with an Oxford Link ISIS system for EDX.

Electrochemical Detection: The electrochemical response was measured at room temperature with a conventional three-electrode system and an electrochemical workstation (Solartron, SI1287). All potentials were referred to a saturated calomel electrode (SCE). Platinum gauze was used as the counter electrode. A modified glassy carbon (GC) electrode (3 mm in diameter) was used as the working electrode. The method of modifying the GC electrode is as follows: a Nafion film alcohol solution (0.5 mL, 1 vol.-%) and the as-prepared gold particles (0.2 mg) were mixed to form a suspension. The suspension (50 μL) was cast onto the surface of the pretreated GC electrode, and the solvent was allowed to evaporate at room temperature, leaving the as-prepared gold immobilized coating on the GC electrode surface. To compare the sensor ability, the same conditions were employed but the working electrodes were changed to a commercial gold electrode and a bare GC electrode with the same diameters.

Supporting Information (see footnote on the first page of this article): Further characterisation and sensing abilities of the Au microflowers.

Acknowledgments

F. Y. thanks the EPSRC for financial support through a grant to R. E. Morris (No. EP/K005499/1). Z. L. thanks the National Natural Science Foundation of China (No. 51302280), Natural Science Foundation of Qinghai (2014-ZJ-936Q), and Young Scholar Project of Qinghai Institute of Salt Lakes, Chinese Academy of Sciences for support. W. Z. thanks the EPSRC for financial support to the Electron Microscopy Laboratory at St Andrews (No. EP/F019580/1). The authors also thank Dr. Chengsheng Ni for help with the electrochemical tests.

[1] X. L. Cui, G. D. Liu, Y. H. Lin, *J. Biomed. Nanotechnol.* **2005**, *1*, 320–327.
[2] S. Komathi, A. I. Gopalan, S.-K. Kim, G. S. Anand, K.-P. Lee, *Electrochim. Acta* **2013**, *92*, 71–78.
[3] a) Y. Zhang, Y. J. Sun, Z. L. Liu, F. G. Xu, K. Cui, Y. Shi, Z. W. Wen, Z. Li, *J. Electroanal. Chem.* **2011**, *656*, 23–28; b) M.-J. Song, S. Hwang, D. Whang, *J. Appl. Electrochem.* **2010**, *40*, 2099–2105.
[4] a) C. X. Lei, H. Wang, G. L. Shen, R. Q. Yu, *Electroanalysis* **2004**, *16*, 736–740; b) X. Yang, F. B. Xiao, H. W. Lin, F. Wu, D. Z. Chen, Z. Y. Wu, *Electrochim. Acta* **2013**, *109*, 750–755.
[5] A. Gutes, I. Laboriante, C. Carraro, R. Maboudian, *Sensors Actuators B* **2010**, *147*, 681–686.
[6] W. Zhao, H. C. Wang, X. Qin, X. S. Wang, Z. X. Zhao, Z. Y. Miao, L. L. Chen, M. M. Shan, Y. X. Fang, Q. Chen, *Talanta* **2009**, *80*, 1029–1033.
[7] K. J. Babu, A. Zahoor, K. S. Nahm, R. Ramachandran, M. A. J. Rajan, G. G. Kumar, *J. Nanopart. Res.* **2014**, *16*, Article 2250.
[8] a) S. Chabi, C. Peng, D. Hu, Y. Q. Zhu, *Adv. Mater.* **2014**, *26*, 2440–2445; b) G. H. Tian, Y. J. Chen, W. Zhou, K. Pan, C. G. Tian, X. R. Huang, H. G. Fu, *CrystEngComm* **2011**, *13*, 2994–3000; c) C. F. Zhang, Z. X. Chen, Z. P. Guo, X. W. Lou, *Energy Environ. Sci.* **2013**, *6*, 974–978; d) X. Yang, Z. Z. Lv, E. K. Wang, X. P. Sun, *J. Electroanal. Chem.* **2011**, *656*, 17–22; e) X. P. Sun, M. Hagner, *Langmuir* **2007**, *23*, 9147–9150.
[9] S. J. Guo, D. Wen, S. J. Dong, E. K. Wang, *Talanta* **2009**, *77*, 1510–1517.

[10] R. Ning, W. B. Lu, Y. W. Zhang, X. Y. Qin, Y. L. Luo, J. M. Hu, A. M. Asiri, A. O. Ai-Youbi, X. P. Sun, *Electrochim. Acta* **2012**, *60*, 13–16.
[11] R. J. Liu, S. W. Li, X. L. Yu, G. J. Zhang, S. J. Zhang, J. N. Yao, B. Keita, L. Nadjo, L. J. Zhi, *Small* **2012**, *8*, 1398–1406.
[12] Y. Chen, X. Gu, C. G. Nie, Z. Y. Jiang, Z. X. Xie, C. J. Lin, *Chem. Commun.* **2005**, 4181–4183.
[13] R. J. Cui, C. Liu, J. M. Shen, D. Gao, J. J. Zhu, H. Y. Chen, *Adv. Funct. Mater.* **2008**, *18*, 2197–2204.
[14] X. Y. Chen, M. H. Qiao, S. H. Xie, K. N. Fan, W. Z. Zhou, H. Y. He, *J. Am. Chem. Soc.* **2007**, *129*, 13305–13312.
[15] Z. L. Wang, R. P. Gao, B. Nikoobakht, M. A. El-Sayed, *J. Phys. Chem. B* **2000**, *104*, 5417–5420.
[16] F. J. Yu, W. Z. Zhou, R. M. Bellabarba, R. P. Tooze, *Nanoscale* **2014**, *6*, 1093–1098.
[17] H. Ataee-Esfahani, M. Imura, Y. Yamauchi, *Angew. Chem. Int. Ed.* **2013**, *52*, 13611–13615; *Angew. Chem.* **2013**, *125*, 13856.
[18] a) M. Pan, S. X. Xing, T. Sun, W. W. Zhou, M. Sindoro, H. H. Teo, Q. Y. Yan, H. Y. Chen, *Chem. Commun.* **2010**, *46*, 7112–7114; b) R. J. Liu, S. W. Li, X. L. Yu, G. J. Zhang, Y. Ma, J. N. Yao, B. Keita, L. Nadjo, *Cryst. Growth Des.* **2011**, *11*, 3424–3431.
[19] A. Umar, S. Lee, Y. H. Im, Y. B. Hahn, *Nanotechnology* **2005**, *16*, 2462–2468.
[20] a) W. Z. Zhou, F. J. Yu, H. F. Greer, Z. Jiang, P. P. Edwards, *Appl. Petrochem. Res.* **2012**, *2*, 15–21; b) J. Zhang, F. J. Shi, J. Lin, D. F. Chen, J. M. Gao, Z. X. Huang, X. X. Ding, C. C. Tang, *Chem. Mater.* **2008**, *20*, 2937–2941.
[21] S. J. Guo, E. K. Wang, *Nano Today* **2011**, *6*, 240–264.
[22] G. Y. Shan, S. J. Zheng, S. P. Chen, Y. W. Chen, Y. C. Liu, *Colloids Surf. B* **2013**, *102*, 327–330.
[23] M. P. Yu, H. T. Sun, X. Sun, F. Y. Lu, G. K. Wang, T. Hu, H. Qiu, J. Lian, *Int. J. Electrochem. Sci.* **2013**, *8*, 2313–2329.
[24] G. H. Jeong, M. Kim, Y. W. Lee, W. Choi, W. T. Oh, Q. H. Park, S. W. Han, *J. Am. Chem. Soc.* **2009**, *131*, 1672–1673.

Received: February 15, 2015
Published Online: May 5, 2015

